Self-propulsion of Small Droplets on Thin Liquid Films

by

Victor Julio Leon

B.S. Mechanical Engineering, Texas A&M University (2017)

Submitted to the Department of Mechanical Engineering
in partial fulfillment of the requirements for the degree of

Master of Science in Mechanical Engineering

at the

MASSACHUSETTS INSTITUTE OF TECHNOLOGY

September 2019

Author Signature redacted

Department of Mechanical Engineering
August 9, 2019

Certified by Signature redacted

Kripa K. Varanasi
Professor of Mechanical Engineering
Thesis Supervisor

Accepted by Signature redacted

Nicolas G. Hadjiconstantinou
Professor of Mechanical Engineering
Chairman, Committee on Graduate Students

Self-propulsion of Small Droplets on Thin Liquid Films

by

Victor Julio Leon

Submitted to the Department of Mechanical Engineering
on August 9, 2019, in partial fulfillment of the
requirements for the degree of
Master of Science in Mechanical Engineering

Abstract

In this thesis, we investigate the self-propulsion of small droplets below the capillary length on thin liquid films. At film temperatures above the boiling point of the droplet and lower film viscosities, we observe that droplets can propel at velocities up to 16cm/s. We predict the droplet velocities using a model that scales thin oil film viscous friction to the momentum of the vapor ejected from beneath the boiling droplet.

Thesis Supervisor: Kripa K. Varanasi
Title: Professor of Mechanical Engineering

Acknowledgements

First, I would like to thank my advisor and mentor, Professor Kripa Varanasi. I have learned so much from him during my 1.5 years in his research group. He has created a great environment for my development as an independent researcher. I am constantly impressed and inspired by Kripa's ability to systematically analyze complex engineering problems and then propose creative solutions. I feel very lucky that I have the opportunity to work with Kripa.

I'd like to thank the members of the Varanasi Research Group. In particular, I'd like to thank Leonid and Henri for mentoring me as senior graduate students in the group. I'd like to thank Vishnu, Jack, Maxime, and Alvaro for the fruitful discussions on experiments and theory we've had regarding these self-propelling droplets and their mentorship. Additionally, I want to thank Sami, Sam, Caroline, Somu, Sreedath, Haeun, Ingrid, Karim, Divya, and Maher. Everyone in the group is very willing to help in any way they can.

I'd like to thank my friends for keeping me sane during the highs and lows these last two years. A non-exhaustive list includes: Scott, Ashley, Zemirah, Andy, Ethan, Joanna, Patricio, Cameron, Tyler, Jackie, Michael, Leilani, Michiko, Yosuke, Anas, Akane, Yan, and Ryan. Without my friends, this thesis would not have been possible.

I'd like to thank my mentors during undergraduate: David Ransom, Luis San Andres, Eric Petersen, and Anibal Morones. They gave me my first opportunities to conduct research. For that I am so grateful.

Finally, I'd like to thank my family for their unwavering support. Gracias Mama, Papa, y Pablo. Siempre me soportan y me escuchan cuando lo necesito. Eben, thanks for your love and support through the years and for being an inspiration. Mama Chela y Papa Julio, siempre me inspiran a ser lo mejor que pueda. Mama Aída, te amo mucho y nos vemos pronto. Papa Víctor, tú me has hablado por los dichos de mi Papa. Gracias.

Contents

List of Figures

List of Tables

1 Introduction

Surfaces that remove and prevent the adhesion of foreign matter have recieved significant attention in the context of self-cleaning, anti-icing, and anti-fouling surfaces [1, 2, 3, 4]. Superhydrophobic surfaces, inspired by natural surfaces like the banana leaf in Figure 1, are considered a promising class of such surfaces because water droplets will capture contaminating particles and roll off with them. However, superhydrophobic surfaces are susceptible to Cassie-to-Wenzel transition, after which a droplet is impaled and immobilized by the surface, and depend on external forces, such as gravity, to move the droplets [5]. Active droplet manipulation has also been explored by using electric, magnetic, and vibrational fields, but such technologies have difficulties with surface pinning and viscous liquids [6].

In this context, systems in which a droplet self-propels are promising avenues to remove contaminants from surfaces, with further applications in lab-on-a-chip technology, ink-jet printing, spray cooling, targeted drug delivery, repellency, and fog collection [7, 8, 9]. Droplet self-propulsion has been shown using ratcheted surfaces, the Marangoni effect, thermal gradients, and electric fields [7, 10, 9, 11]. In this thesis, the phenomena of self-propulsion of droplets on thin liquid films is explored experimentally, and a model is developed to predict the observed droplet velocities. To the author's best knowledge, this phenomena has not been studied before.

Figure 1: A natural, superhydrophobic banana leaf. Droplets easily slide off and take dirt particles with them.

2 Background

2.1 Previous work on self-propelling droplets

Droplet self-propulsion has been demonstrated in numerous ways. Linke et al. showed that the Leidenfrost effect can be used in conjunction with a ratchet substrate to propel droplets at velocities ca. 10cm/s on millimetric ratchets [7]. Lagubeau et al. observed that, for the droplets to propel, the droplets must be larger than the wavelength of the ratchet [12]. Using micro- and nano-metric ratchet textures, Ok et al. demonstrated maximum velocities ca. 40cm/s, with the smallest droplets observed being of radius 0.89mm [13]. The main disadvantages of the ratchet propulsion method are the time consuming manufacturing methods required to create the ratcheted surfaces.

Another class of methods that self-propel droplets use Marangoni induced motion. Izri et al. showed the self-propulsion of droplets with radii 20-60μm, reporting velocities in the range 10-50μm/s due to a concentration gradient of surfactants around a droplet [10]. Bormashenko et al. observed liquid marbels propelling at velocities ca. 10cm/s as a result of condensation of alcohol from the liquid marbel on the water surface [8]. The disadvantages of this method are the inability to control the direction of propulsion and the necessity to modify the droplets with contaminants.

Thermocapillary effects have been explored as a means of self-propulsion. On conventional solid surfaces, large temperature gradients are required for velocities ca. 1mm/s due to surface pinning forces [14]. Bjelobrk et al. eliminated pinning by using lubricant infused surfaces in which the droplet is separated from the surface by a thin oil layer, resulting in millimetric droplets with velocities of up to 6.5mm/s for thermal gradients of 2K/mm [9]. In order to ensure that a thin oil layer remains between the substrate and the droplet, careful selections of oil, surface texture, and surface properties are required.

Gunji et al. used AC and DC electric fields of ca. 300V to propel distilled water droplets of volume 1.5 μL at velocities as high as 10cm/s [11]. The observed droplet motion is due to a thin layer of water left behind by

the advancing droplet, leading to an imbalance in the Maxwell stress. The droplet is placed on a surface with two electrodes covered by hydrophobic insulation.

As can be seen, most methods of self-propulsion require the labor intensive modification of the surface or of the droplet. The phenomena of self-propulsion on thin liquid films explored in this thesis requires neither and can achieve competitive velocities, ca. 10cm/s, by applying a thin oil coating onto a surface.

2.2 Relevant fundamentals of interfacial phenomena

The system of interest has four pertinent phases: the solid surface, the thin oil film, the droplet, and air. Analysis of how the four phases will interact depends on knowledge from the field of interfacial phenomena. Topics relevant to the experiments conducted will be discussed here. For a more detailed coverage of interfacial phenomena, see the textbook by de Gennes et al. [15].

2.2.1 Young-Laplace equation

A basic system to consider is one composed of two immiscible liquids. An example of such a system is a bubble of air surrounded by water. For simplicity, consider a situation in which the bubble and surrounding liquid are stationary and have the same density. The bubble will take the shape of a sphere in order to minimize its surface area. Due to surface, or interfacial, tension, there will be a pressure rise at the interface where the two phases meet. The pressure rise is described by the Young-Laplace equation where γ is the interfacial tension between the bubble and the liquid and R_1 and R_2 are the radii of curvature of the bubble surface:

$$\Delta P = \gamma \left(\frac{1}{R_1} + \frac{1}{R_2} \right) \tag{1}$$

2.2.2 Young equation

The Young equation relates the contact angle of a liquid droplet on a solid surface surrounded by a vapor with the interfacial tensions between each of the phases (s-solid, l-liquid, and v-vapor) [15].

$$\gamma_{lv} \cos\theta = \gamma_{sv} - \gamma_{sl} \tag{2}$$

For a given solid-liquid-vapor combination, the contact angle can have any value from 0° to 180°. The four main categories of liquid wettability on a surface are shown in Figure 2. A liquid with a contact angle of 0° is called a fully wetting liquid. A fully wetting liquid will spread until it completely covers the solid surface if there is enough liquid and time to do so. A liquid with a contact angle of 180° is called a non-wetting liquid.

In reality, even the smoothest surfaces have micro and nano scale roughness and impurities. Although the Young equation is always satisfied, the macroscopic effect of the defects is a difference between the advancing (θ_a) and receding (θ_r) contact angles. Contact angle hysteresis is defined as $\Delta\theta = \theta_a - \theta_r$. Contact angle hysteresis is the cause of the pinning of droplets on surfaces.

2.2.3 The four phase system

Analysis of the system studied in this thesis is complicated because it is composed of four phases, with all of their associated interfaces. Fortunately, the system has been comprehensively studied thermodynamically in literature in the context of lubricant infused surfaces (LIS) [16].

In this thesis, the surface tension between two phases will be denoted as γ_{ij}, where i and j can be any combination of s (solid), w (water), o (oil), and a (air) as long as $i \neq j$. For example, γ_{wo} is the interfacial tension between the oil and water.

Of particular importance to the behavior of a droplet self-propelling on a thin, oil film is whether the oil tends to spread over, or cloak, the droplet; this is determined by the spreading coefficient of the oil on water in air,

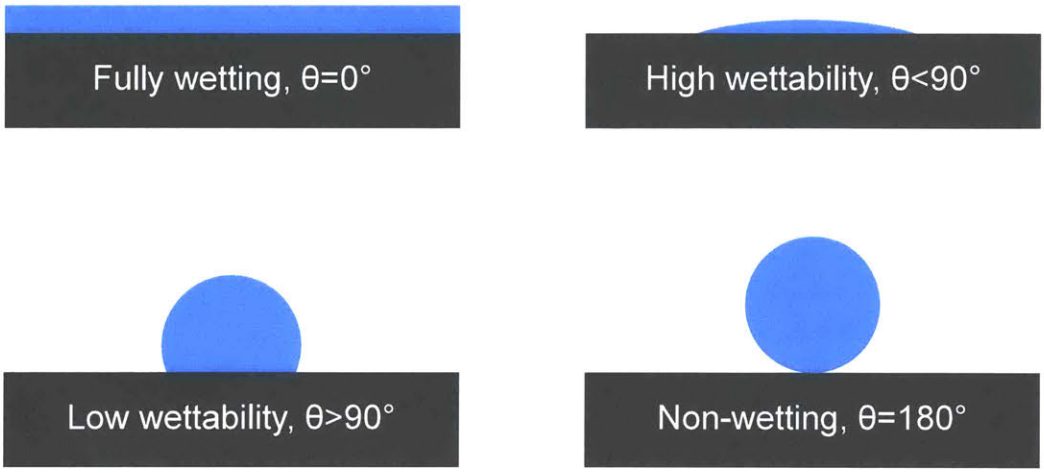

Figure 2: The four main categories of liquid wettability on a surface.

$S_{ow(a)} = \gamma_{wa} - \gamma_{wo} - \gamma_{oa}$. The oil will tend to cover the droplet only if $S_{ow(a)} > 0$. Here, $S_{ow(a)}$ is evaluated at 100°C because the temperature of the outer surface of the droplet cannot exceed the boiling point of water at atmospheric pressure. At 100°C, γ_{wa} is 58.9mN/m. The relevant oil interfacial tensions and spreading coefficients at elevated temperatures for the two oils studied, Krytox GPL 107 and silicone oil, are tabulated from literature in Table 1 [9, 17, 18, 19, 20]. As can be seen, silicone oil is expected to be spreading, whereas Krytox is expected leave the droplet uncloaked at 100°C. Although the γ_{wo} for Krytox is measured at room temperature, it is not expected to change significantly with temperature, similarly to that of silicone oil. This assumption is discussed in the experimental results section.

The behavior of the oil film under the droplet is of critical importance, too. An oil will infuse a textured, solid surface and be considered an LIS if

$$\theta_{os(a)} \leq \theta_c \tag{3}$$

Liquid	γ_{oa}	γ_{ow}	$S_{ow(a)}$
Silicone Oil	13.8	40	5.1
Krytox GPL 107	17	57.2	-15.3

Table 1: Interfacial tension and spreading coefficient values from literature at or near 100°C. All values are reported in mN/m. The oil will cloak the droplet only if $S_{ow(a)} > 0$.

$$\theta_c = cos^{-1}\left(\frac{1-\phi}{r-\phi}\right) \tag{4}$$

where $\theta_{os(a)}$ is the contact angle of oil on the smooth solid surface in the presence of air and θ_c is the critical contact angle for infusion [16]. ϕ is the fraction of projected area of the textured surface occupied by solid and r is the ratio of total surface area of the textured surface to its projected area. For the square post surfaces used in experiments,

$$\phi = \frac{a^2}{(a+b)^2} \tag{5}$$

$$r = 1 + \frac{4ah}{(a+b)^2} \tag{6}$$

where a is the post side length, b is the edge-to-edge spacing, and h is the post height. Critically, infusion of the texture does not guarantee that the post tops will be covered by oil in air. For the oil to cover the post tops, the oil must fully wet the solid ($\theta_{os(a)} = 0°$). With the water drop introduced, one must also consider $\theta_{os(w)}$ in place of $\theta_{os(a)}$ in the above conditions in order to ensure that the oil will remain infused under the drop and that an oil film will remain between the water droplet and the post tops.

The behavior of the oil film in the textures and on the post tops under water is particularly relevant for experiments conducted in this thesis. As mentioned above, the main cause for droplet pinning on a surface is $\Delta\theta$, and $\Delta\theta$ is caused by surface defects and impurities. Ensuring that an oil film is

between the droplet and solid surface can minimize pinning and provide a defect-free, liquid-liquid interface for the droplet to slide over.

3 Self-propulsion of small droplets on thin liquid films

3.1 Experimental setup

Figure 3 shows a schematic of the experimental setup. Surface samples are placed with thermal paste on a steel plate to ensure good thermal contact and a homogenous temperature distribution on the sample surface. Surface temperature is measured with a Type-K thermocouple and adjusted by using hotplate controls to within $\pm 3°C$. An optical stage is used to adjust the vertical distance between the syringe and the sample surface. Droplets are gently deposited from a height of about one diameter from the surface. DI water at room temperature is pushed out of a 27G stainless steel needle at a rate of 0.07mL/min by a syringe pump. The 27G needle dispenses droplets with radii near the capillary length ($\sim$1.2mm).

A Photron FASTCAM SA 1.1 was used to record the droplets. To observe boiling phenomena, droplet videos at 100,000fps were taken with the camera line of sight parallel to the substrate surface. Diffuse light was used to image the bottom of the droplet. Direct light from a high power LED light was used to image the edge of the droplet. Most videos at 5,400fps to measure droplet velocity were taken from above at approximately 45° with respect to the substrate. Sample surfaces were leveled using a spirit level. All velocity values reported are the average of 4-6 experiments. Reported error bars are the standard deviations of the experiments. Silicone oils with 100, 500, and 1,000cSt viscosities at room temperatures were used in the following studies. Krytox and silicone oil film viscosities at elevated temperatures were calculated using manufacturer equations and data [21, 22].

Experiments in this study were carried out using flat silicon or lubricant infused surface (LIS) substrates. The LIS were made using methods described in literature to ensure that the surface's texture would be infused by silicone oil and that there would be a thermodynamically stable oil film between the DI water droplet and the post tops [16]. Specifically, all of the LIS used in our experiments were silicon surfaces with 10x10μm square top posts with 5μm edge-to-edge spacings, as shown in Figure 4, and heights of 7μm functionalized with octadecyltrichlorosilane (OTS) and infused with silicone

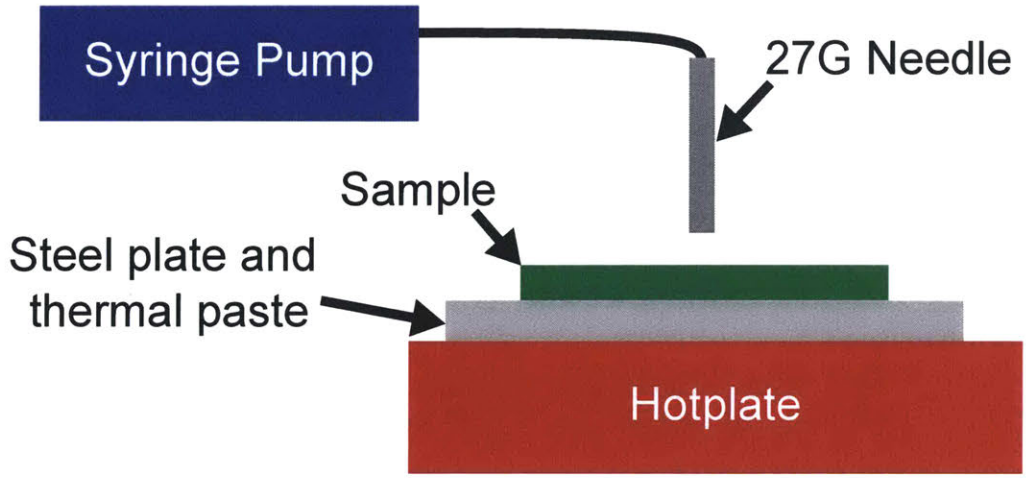

Figure 3: A schematic of the experimental setup.

oil.

Silicon surfaces were textured using deep-reactive-ion etching (DRIE) in combination with common photolithographic techniques. The textured surfaces were then coated with OTS by solution deposition. The samples were infused with silicone oil by dipcoating them at velocities V such that $Ca = \mu V/\gamma_{oa} < 10^{-4}$ to ensure that no excess oil would be on the post tops [23].

The flat silicon substrates were functionalized to ensure that the tested oil would fully spread on the surface. Flat silicon surfaces for use with Krytox were functionalized using Dupont Teflon AF following manufacturer instructions [24]. Although Krytox does not fully wet Teflon surfaces under water, it has been observed that water droplets at 95°C oleoplane on oil films above Teflon surfaces [20, 25]. Flat silicon surfaces for use with silicone oil were functionalized with silicone oil using techniques from literature, where it was found that inorganic oxide surfaces can be chemically modified by the addition of silicone oil at temperatures above 100°C [26, 27]. 100,000fps videos were taken on a flat stainless steel surface that was similarly functionalized with silicone oil. The silicone oil films for the 100,000fps experiments were spread with a razor blade.

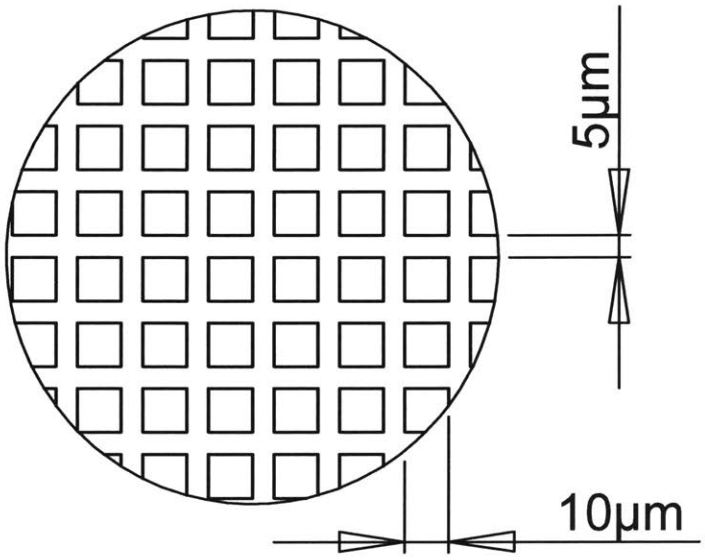

Figure 4: Schematic showing the arrangement of the square posts and how post edge-to-edge spacing is defined.

The thicknesses of the spincoated silicone oil films on the surfaces were estimated using theory, which has been shown to predict the thickness of spincoated PDMS films [28, 29]. According to theory, the thickness, h, of a spincoated film is given by

$$h = \frac{h_0}{\sqrt{1 + 4Kh_0^2 t}} \tag{7}$$

$$K = \frac{\rho\omega^2}{3\mu} \tag{8}$$

where h_0 is initial film thickness, t is spincoat time, ρ is the liquid's density, ω is radial velocity, and μ is the liquid's viscosity.

3.2 Experimental results and discussion

Figure 5 shows the observed difference in droplet behavior between a normal silicon surface, a silicon surface hydrophobized by silicone oil, and silicon surface with a thin, spreading oil film that was spincoated. The droplet on the normal silicon surface boils then bounces on the surface with Leidenfrost like behavior. The droplet on the hydrophobized silicon surface goes directly to the Leidenfrost state. In both cases, the droplet moves and accelerates slowly, with minimal movement seen between the successive images.

The droplet on the spincoated oil film exhibits markedly different behavior. After an initial transient stage where the droplet heats up from room temperature (22°C) to its boiling point, the droplet quickly accelerates and propels to the right. Figure 6 shows that droplet symmetry is broken with bubbles forming and ejecting on one side of a propelling droplet. Suprisingly, Figure 7 demonstrates that the droplets reach a steady velocity after about 10ms of acceleration.

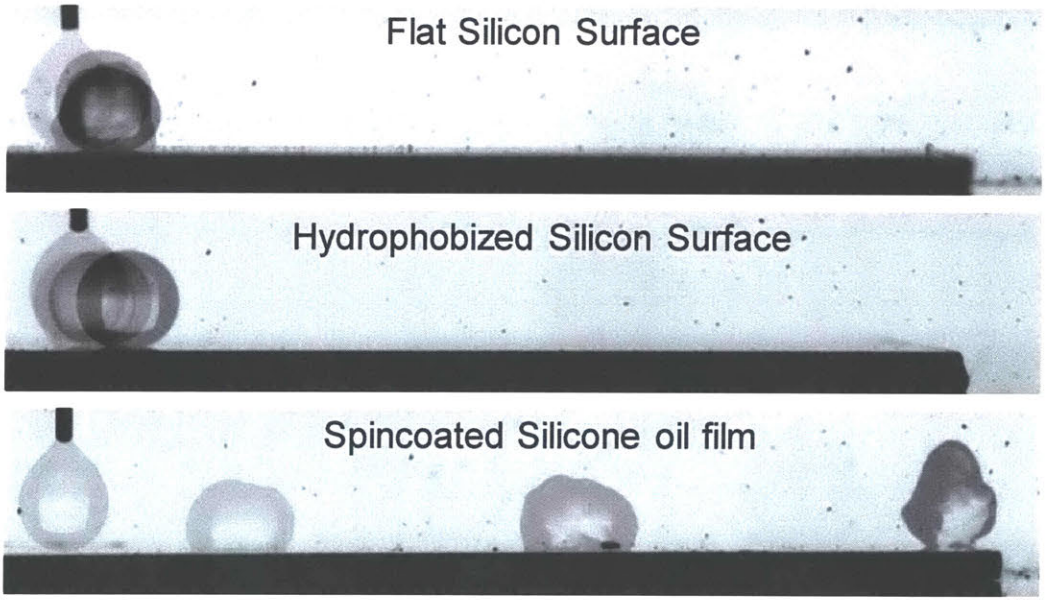

Figure 5: Chronophotography of water droplets on different surfaces at 180°C. Each successive image is taken after 100ms. The outer diameter of the syringe in the top left corner of each image is 0.4128mm.

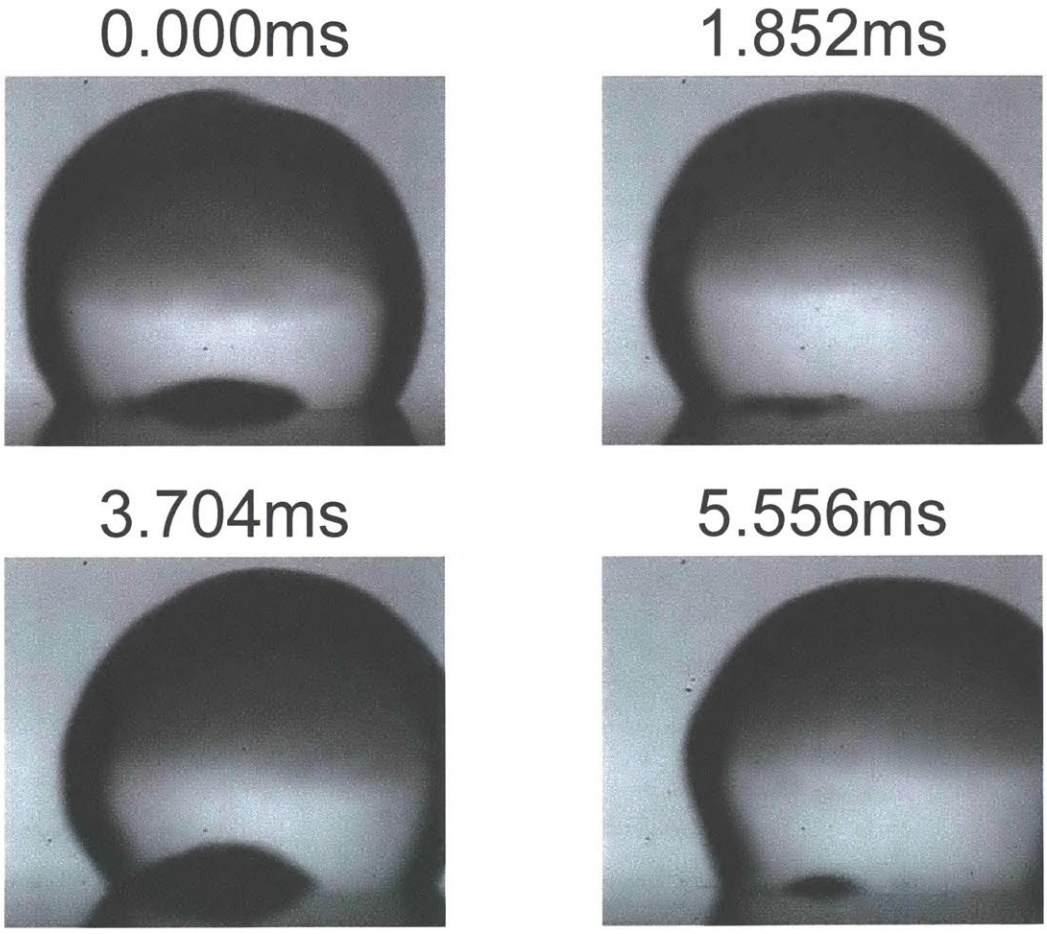

Figure 6: Droplet propelling on a spincoated silicone oil film of viscosity 15mPas at 160°C demonstrating typical asymmetry. The droplet radius is 1.2mm. The droplet is propelling to the right, and vapor bubbles only form and eject from the left side of the droplet.

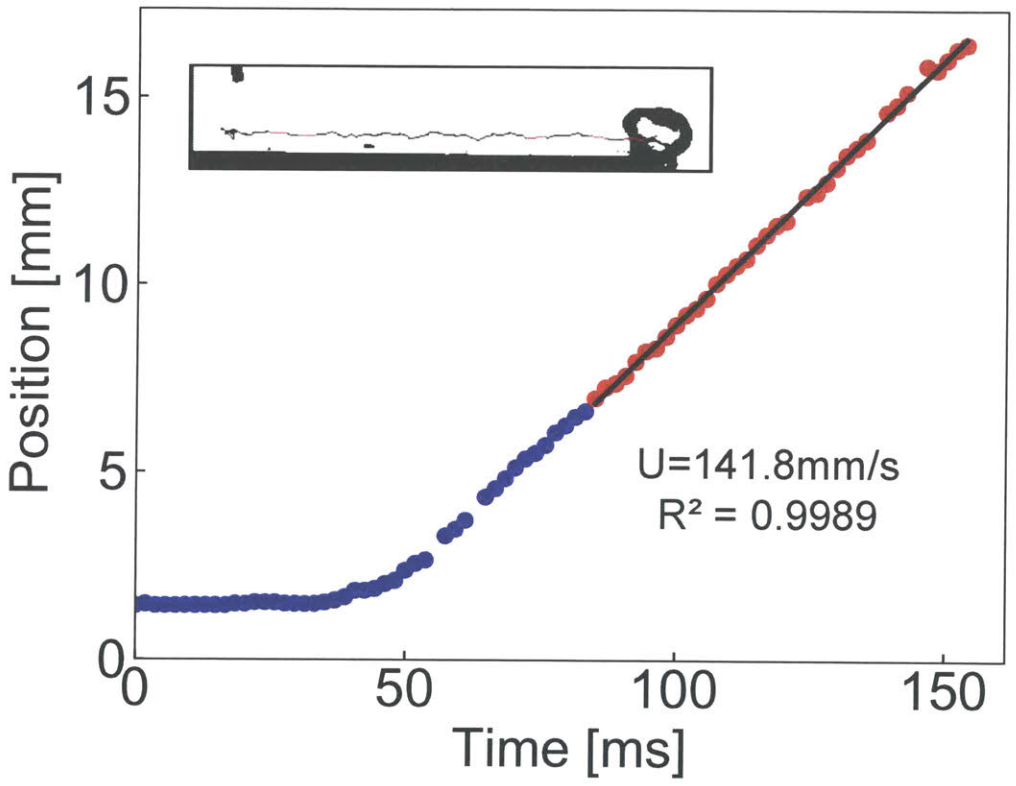

Figure 7: Droplet position vs time on an LIS infused with oil of viscosity 15mPas at 160°C. Inset shows detected path. Red markers show where the linear fit, denoted as a solid black line, is taken to determine velocity.

The difference between a cloaking and non-cloaking oil was pronounced. As discussed in the background section, Krytox is not expected to cloak the water droplet, while silicone oil is expected to cloak the droplet. Propulsion experiments conducted on Krytox films resulted in droplets repeatedly making small, vertical jumps. In comparison, droplets on silicone oil films were kept close to the surface and rarely, if ever, completely separated from the surface. Ultimately, this resulted in the droplets on silicone oil propelling smoothly, as opposed to the slow and sporadic movement on Krytox. Additionally, after multiple droplet experiments at the same spot on a silicone oil film, a dry patch was observed on the surface. No such dry patch appeared on the Krytox films after multiple droplet experiments. Clearly, whether the oil tends to spread over the droplet is a critical property in the behavior of the system.

The effect of oil film thickness on droplet velocity is shown in Figure 8. In the extreme case of a pool of oil, the droplet fully sinks into the pool. Since there is liquid-liquid contact, few, if any, nucleation sites exist at the interface. This allows the droplet to superheat, leading to vapor explosions [30]. As the thickness reaches the height of the droplet, a wetting ridge forms. However, at this height, the ejection of vapor is completely blocked by the large wetting ridge. Droplets are observed to remain stationary until a vapor explosion occurs. One such vapor explosion is shown in Figure 9. As film thickness lowers, the wetting ridge size decreases, as confirmed by Figure 10 and literature [31, 32]. The first observable, regular velocity is at 15μm. Below 7μm, it is observed that droplet velocity loses its dependence on film thickness.

The effect of viscosity on droplet velocity is shown in Figure 11. Velocity appears to be independent of substrate which is expected for a spreading oil film under the droplet [16]. Velocity seems to scale as $\mu^{-0.5}$. Experiments were conducted with droplet sizes of ~1.2mm. Exploding droplets allowed for a few observations below this droplet size. The smallest droplet observed had a radius of 0.3mm, and the largest had a radius of 1.6mm. Droplet size was not observed to have a significant effect on velocity in this range of radii. It should also be noted that the contact area between the droplet and the oil film varies widely between droplet experiments and even within the same experiment due to boiling. Experiments seem to indicate that the velocity of the droplet is not significantly influenced by geometric factors, but is a

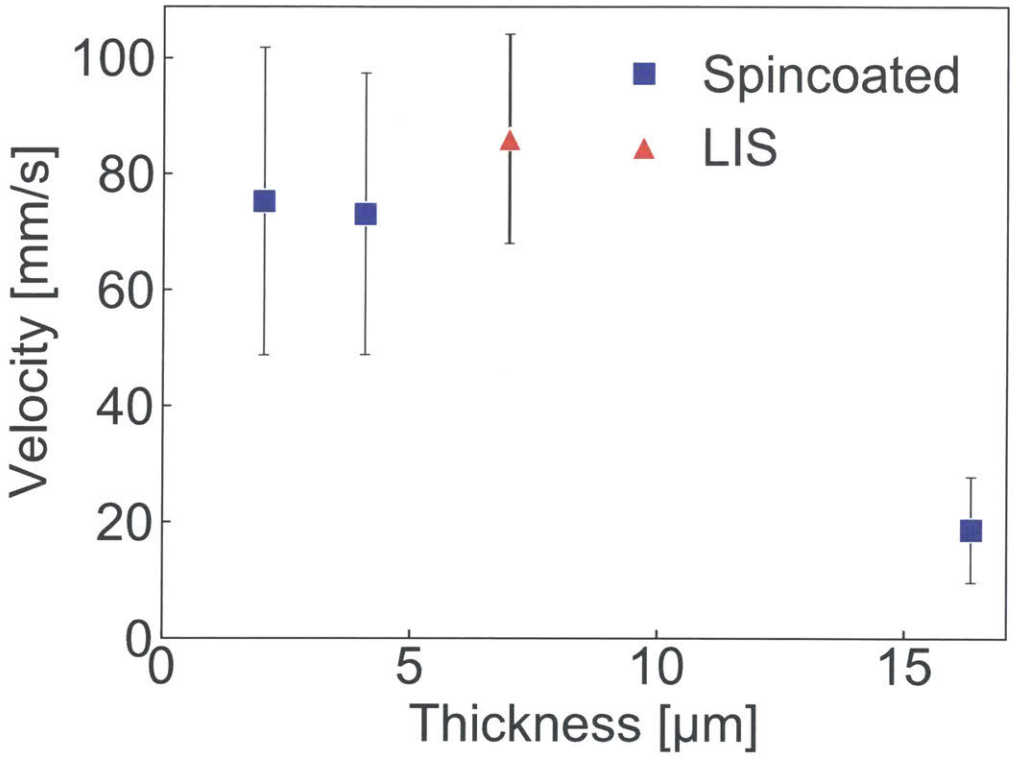

Figure 8: Droplet velocity vs film thickness experiments on 19mPas spin-coated silicone oil at 140°C.

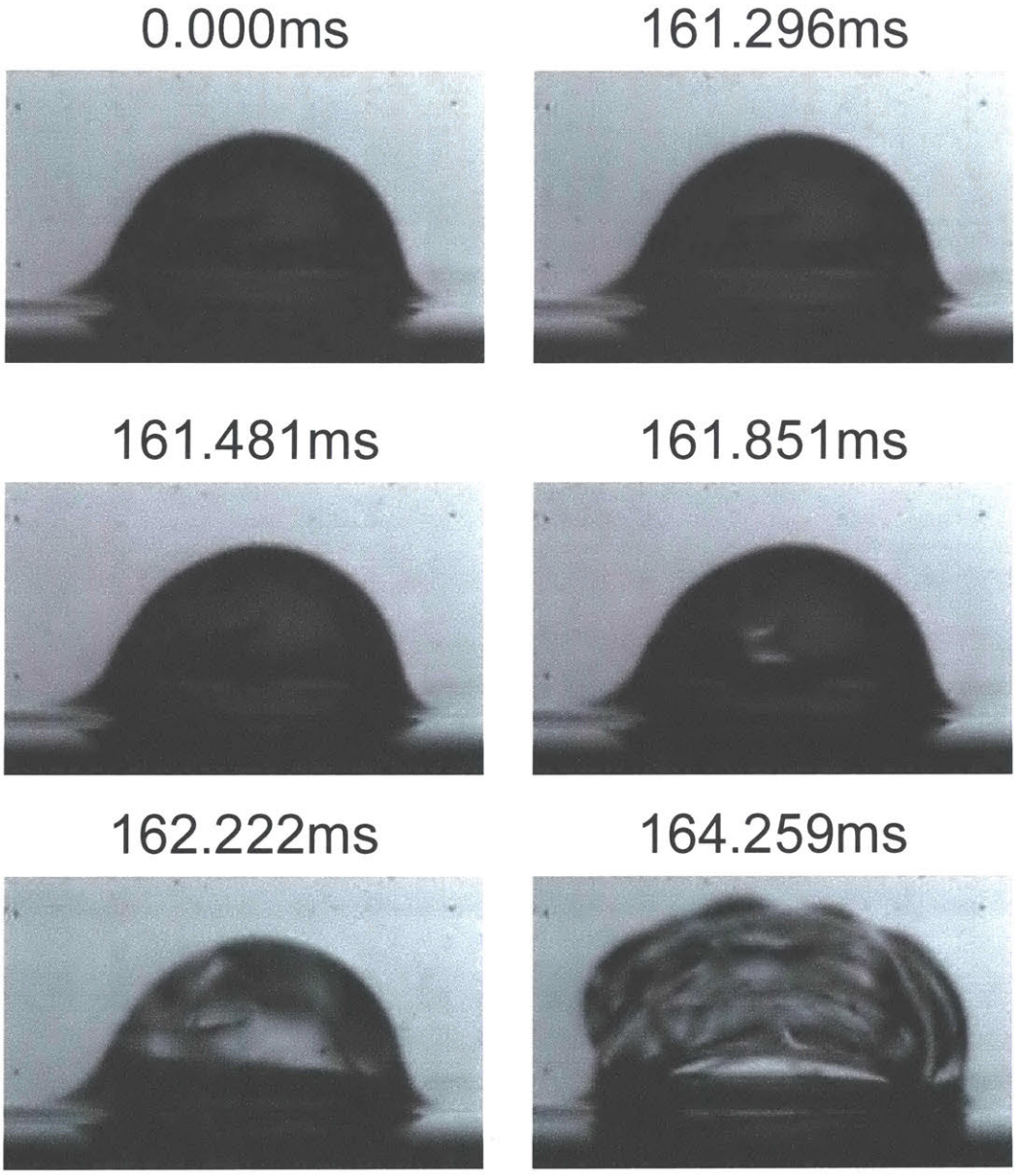

Figure 9: A sequence of images from a video of a vapor explosion on a thick, spincoated silicone oil film at 160°C. Droplet radius is 1.2mm. Homogenous nucleation is evident because the vapor nucleates in the middle of the droplet.

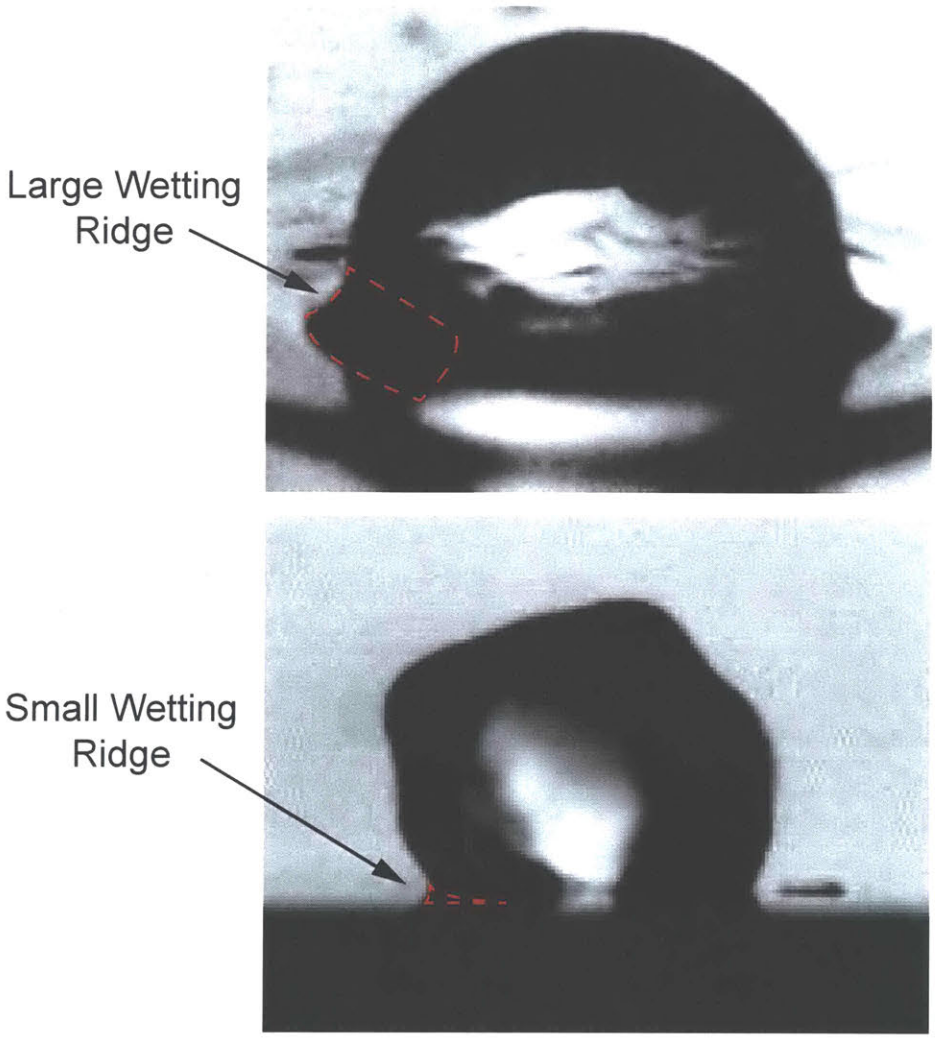

Figure 10: A large wetting ridge observed on a 23μm film and a small wetting ridge observed on LIS. Both droplets have radius 1.2mm. Red dashed lines are guides for the eye.

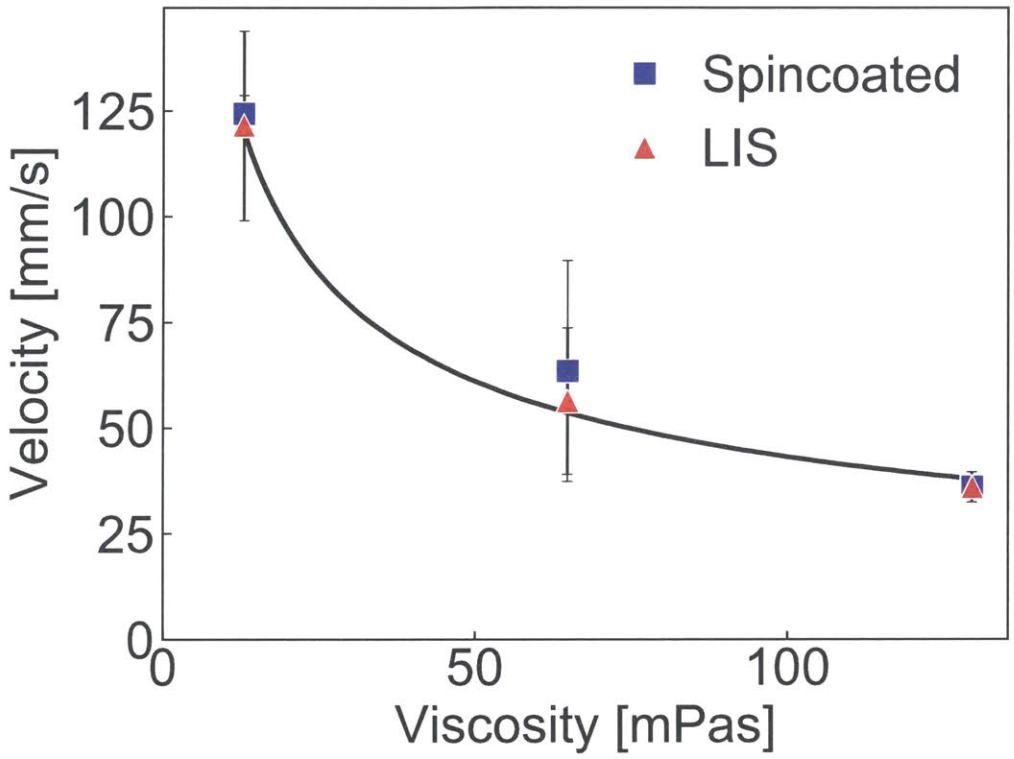

Figure 11: Viscosity vs velocity at 180°C for two different surfaces. The black line corresponds to $U \sim \mu^{-0.5}$.

function of viscosity.

The proposed model scales ejected vapor momentum to viscous dissipation in the oil film, similarly to a propelling rocket. A schematic of the model is depicted in Figure 12. Here, U is the velocity of the droplet and V is the ejected vapor velocity.

$$\frac{\dot{dp}}{dt} \sim F_{film} \tag{9}$$

$$\frac{\dot{dp}}{dt} = \dot{m}V \tag{10}$$

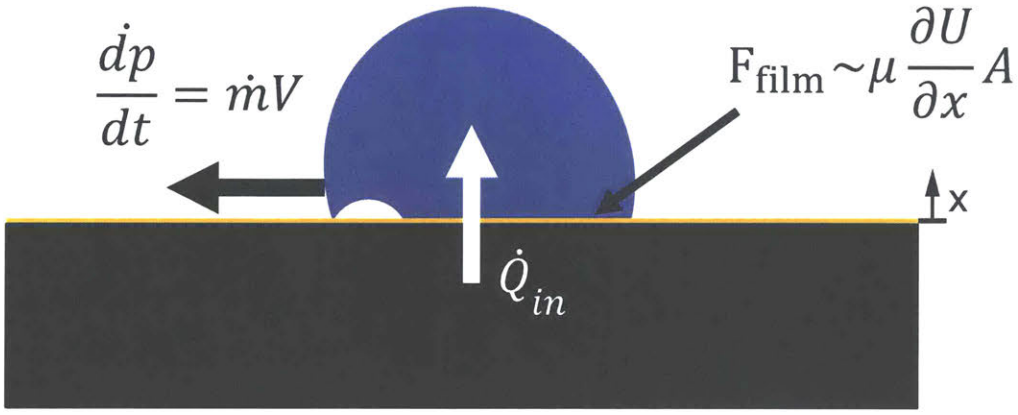

Figure 12: A schematic of the proposed model.

$$F_{film} = \mu \frac{\partial U}{\partial x} A \tag{11}$$

A is the area of contact between the droplet and the oil film. Assuming that the majority of heat into the droplet is used to evaporate the droplet while the droplet is propelling after the initial heating stage,

$$\dot{Q}_{in} = k \frac{\partial T}{\partial x} A \sim \dot{m} h_{fg} \tag{12}$$

h_{fg} is the latent heat of vaporization. The momentum balance will then be as follows:

$$k \frac{\partial T}{\partial x} \frac{1}{h_{fg}} V \sim \mu \frac{\partial U}{\partial x} \tag{13}$$

We are interested in solving for U. The three remaining unknowns are the gradient of U in the oil film, the gradient of T at the oil-droplet interface, and the vapor velocity V.

The order of magnitude V of the vapor ejected from below the droplet is estimated by the curvature of a typical bubble as it is about the eject, as in Figure 13. The pressure within the bubble can be calculated using the

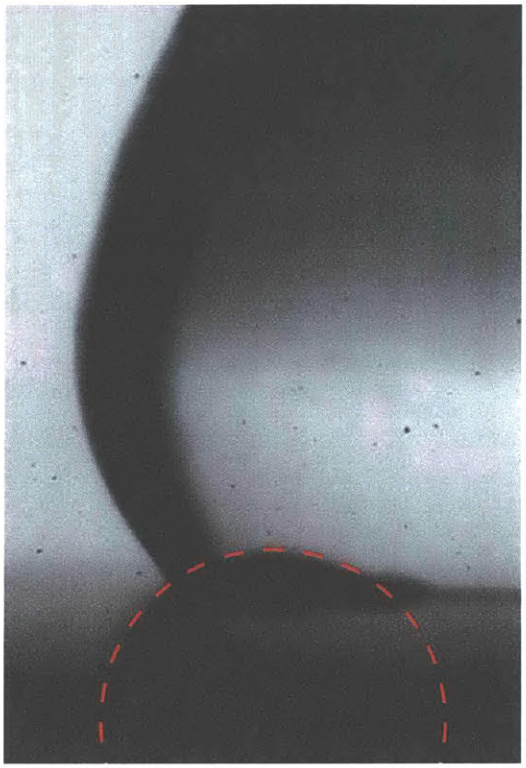

Figure 13: Image showing a typical bubble just before ejection. The sample is LIS with 15mPas silicone oil at 160°C. The drawn circle has radius 0.73mm, corresponding to 25m/s ejection velocity.

Young-Laplace equation. Two main contributions are considered: ΔP from the environment to the interior of the droplet is calculated to be 98Pa using the droplet radius of 1.2mm and γ_{wa}=58.9mN/m and ΔP from the droplet to the inside of the bubble is calculated to be 107Pa using the measured bubble radius of 0.73mm. The total ΔP between the interior of the bubble and the surroundings is approximately 205Pa. Bernoulli's equation can be used to obtain a first approximation of the vapor velocity due to the pressure differential.

$$\Delta P = 0.5\rho V^2 \tag{14}$$

The calculated velocity is 26m/s. It should be noted that the calcu-

lated velocity does not change significantly with bubble radius between 0.5 and 10mm. The corresponding velocities are 29 and 19m/s respectively. V=25m/s is used in calculations from here forward.

$U \sim \mu^{-0.5}$ implies that momentum diffusion through the oil film is significant. Both T and U gradients at the droplet interface can be estimated using diffusion of the respective boundary layers into the oil film. The boundary layer thicknesses scale as

$$\delta_{cond} \sim \sqrt{\alpha\tau} \sim \sqrt{\frac{k}{c_p\rho}\tau} \tag{15}$$

$$\delta_{mom} \sim \sqrt{\nu\tau} \sim \sqrt{\frac{\mu}{\rho}\tau} \tag{16}$$

Setting δ_{cond} and δ_{mom} equal to the characteristic film thickness in experiments, 10μm, the timescale for complete diffusion through the oil film is approximately 1ms for the thermal boundary layer and 1μs for the momentum boundary layer in the case of the most viscous 100mPas oils used. The film thickness under the propelling droplet is expected to be equal to or greater than the initial film thickness as droplets have been observed to oleoplane on thin oil films [25]. This indicates that a phenomena that resets the thermal and momentum boundary layer could be occuring at the 1μs timescale under the droplet.

Observation of the phenomena is inhibited by the rapid rate at which viscosity damps high frequency oscillations [33, 34]. 100,000fps videos taken of a boiling droplet on a 19mPas silicone oil film spread on a steel plate as a thin film by a razor blade at 140°C reveal that fast bubbling events at the oil-water contact occur and can cause droplet surface fluctuations with periods at least in the 10μs timescale. Large bubbles are observed to be stationary under a moving droplet, indicating that bubble formation can stop the movement of the oil film and reset the momentum boundary layer. The thermal boundary layer is reset by the bubble because bubble formation will significantly reduce the heat transferred from the oil film. Additionally, the droplet is always moving over fresh, hot oil.

First, the lighting was set in order to visualize the bottom of the drop.

The high frame rate limits visibility into the droplet, but at moments, a small part of the bottom of the droplet is visible. Figure 14 shows a few frames during one such moment in a 100,000fps video in which multiple surface fluctuations occur within the span of one frame. The oscillations were not observed in videos of Leidenfrost droplets over bare, hydrophobized steel surfaces as seen in Figure 15. The absence of the fluctuations in the case of the Leidenfrost droplet indicates that that the fluctuations are caused by the boiling.

To clarify the frequency of bubbling and highlight the difference between a heated Leidenfrost droplet and a boiling droplet, spatiotemporal diagrams of each case, shown in Figures 16 and 17, were created from a line of pixels on the droplets. Figure 16 used pixels from a horizontal line near the base of the droplet. Figure 17 used the line of pixels indicated by the transparent, dashed red line. Notably, in Figure 16, oscillations caused by the fast boiling at the center of the drop do not have a significant effect on the movement of the edge, as would be expected due to viscous damping of high frequency oscillations.

Figure 18 plots the image intensity values along the red dashed lines in Figures 16 and 17. This is equivalent to sampling the intensity of one point in the droplet over time. A comparison of the image intensity values shows that the very small oscillations in the boiling case can be attributed to sampling noise, but that the larger oscillations are probably caused by fast boiling events under the droplet. As can be seen, bubbling and surface fluctations phenomena appear to occur at least on 10μs timescales. It is expected that as temperature is increased, high frequency bubbling events under the droplet will occur more frequently and more violently.

Figure 19 is a spatiotemporal diagram of a slice near the bottom of a propelling droplet with lighting that accentuates the edge of the droplet. Small and rapid surface fluctations are captured. Blurring of the edge can also be seen near these rapid fluctuations, suggesting phenomena are occuring at frequencies outside of our recording capabilities. Oscillations can be seen to occur in the middle of the droplet that appear decoupled from the oscillations observed on the edge. Again, this can be attributed to the viscous damping of high frequency oscillations.

Information from the videos of the bottom and edge of the droplet indicate

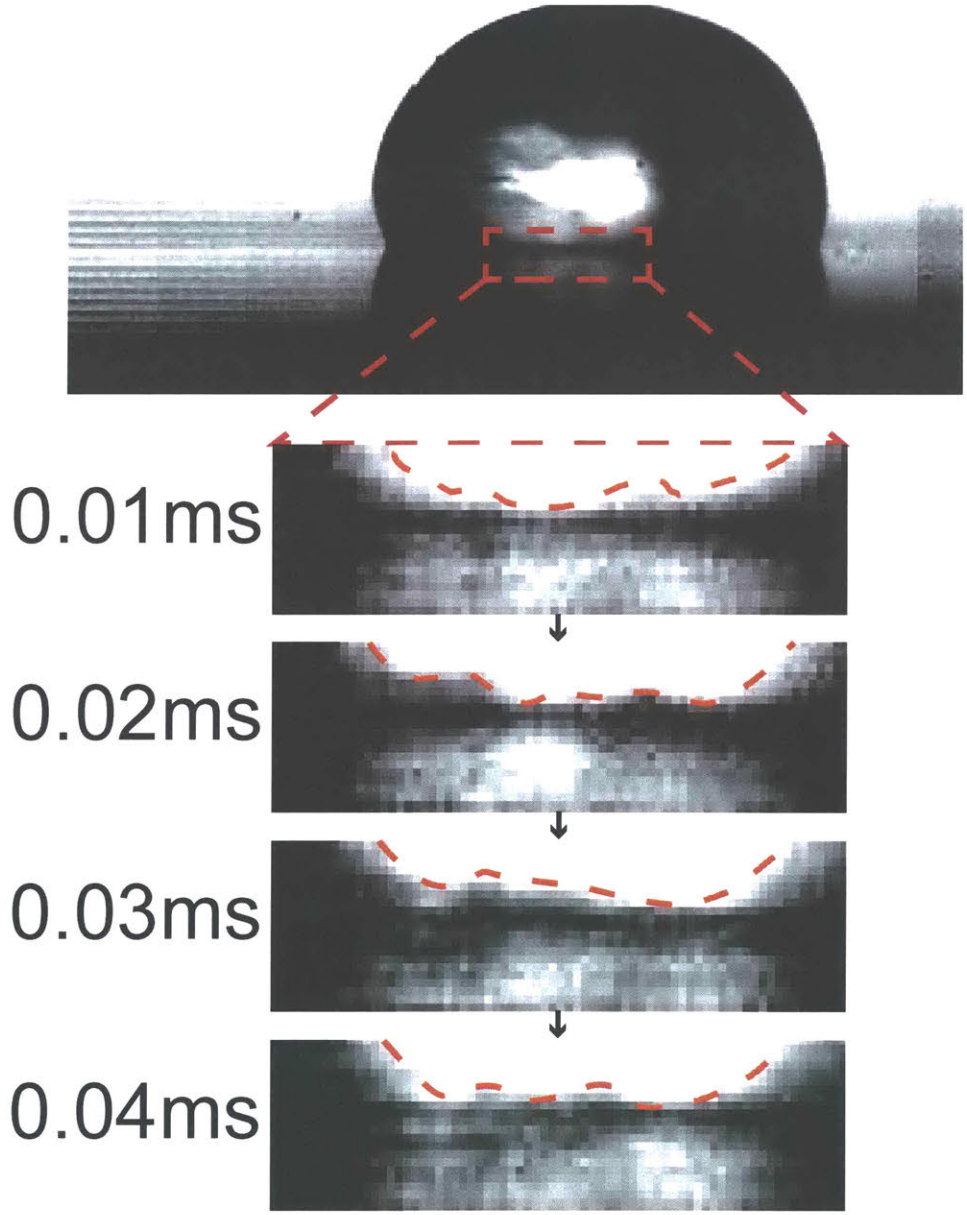

Figure 14: Images from a 100,000fps video of a boiling droplet on a thin, 19mPas silicone oil film spread by a razor at 140°C on a steel plate. Droplet radius is approximately 1.3mm. Zoomed in images at the bottom have contrast increased to highlight the fluctuations observed at the base of the droplet. The dashed orange lines are guides for the eyes.

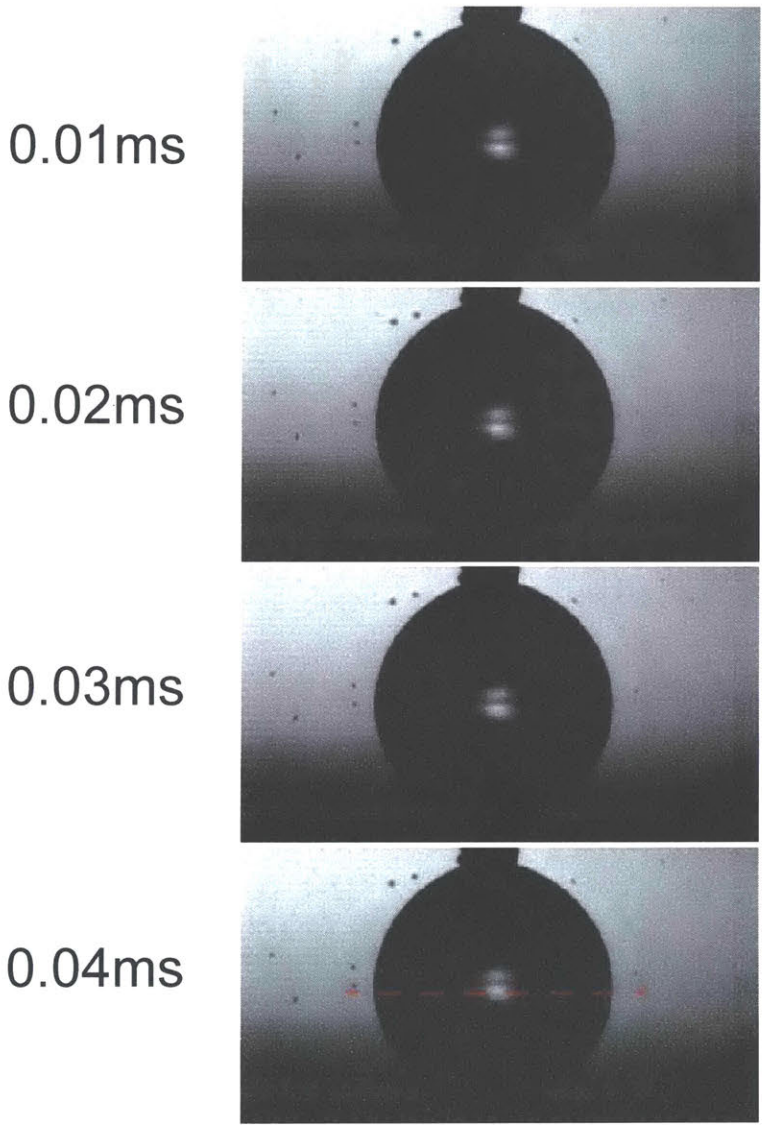

Figure 15: Images from a 100,000fps video of a Leidenfrost droplet of radius 1.2mm on a thin, 19mPas silicone oil film spread by a razor at 140°C on a steel plate. The droplet is held in place by a needle. The dashed red line shows where the slice was taken for the spatiotemporal diagram in Figure 17.

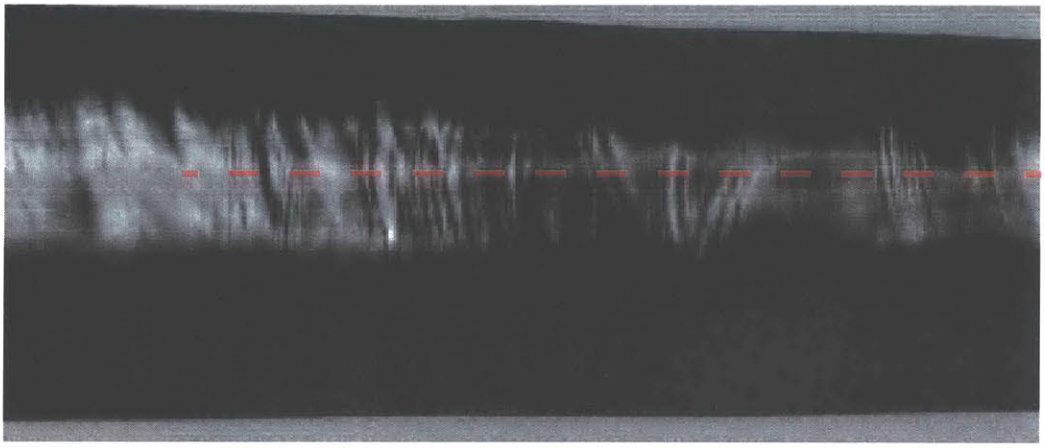

Figure 16: Spatiotemporal diagram of a horizontal slice of pixels from near the base of the boiling droplet shown in Figure 14. The dashed red line shows where the image intensities were taken for Figure 18.

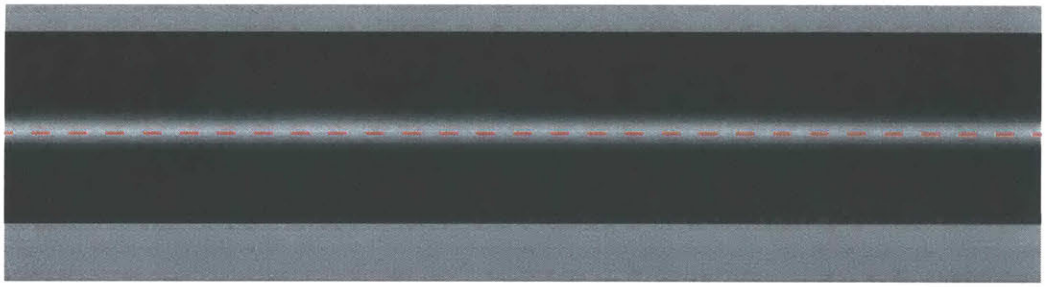

Figure 17: Spatiotemporal diagram of a horizontal slice of the video of the Leidenfrost droplet in Figure 15. The dashed red line shows where the image intensities were taken for Figure 18.

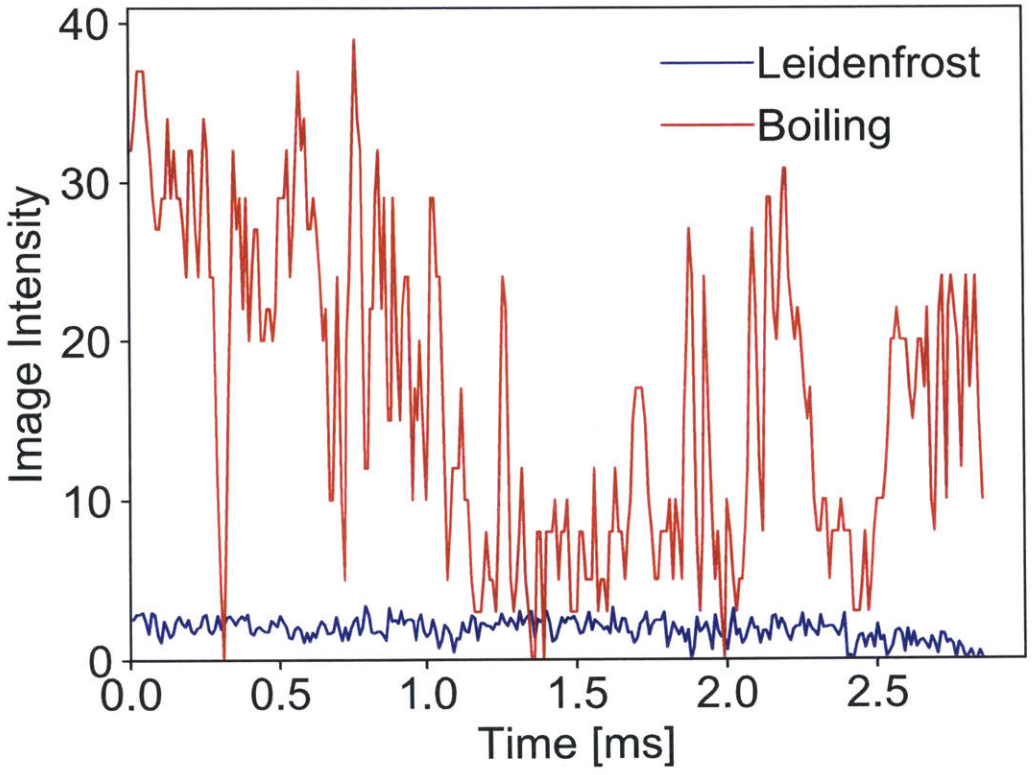

Figure 18: Image grey value taken along the dashed red lines in Figures 16 and 17. The large fluctuations in the boiling image intensity correspond to wrinkles on the surface of the droplet, which are caused by boiling. The smaller fluctuations can be attributed to noise that can also be seen in the Leidenfrost curve.

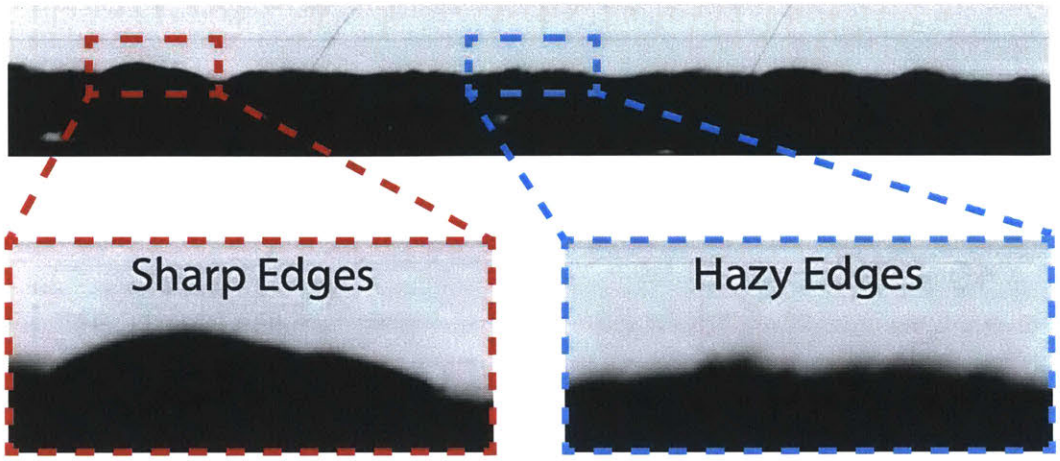

Figure 19: Spatiotemporal diagram from a slice near the bottom of a propelling droplet taken with lighting that accentuates the edge of the droplet. The black area is the droplet. Each horizontal pixel is 10μs. The total length of the spatiotemporal diagram is 1095 pixels or 10.95ms. High freqency oscillations are visible intermittently. The hazy edges indicate that some surface fluctuations occur outside of our recording capabilities.

that fast boiling events are occuring at the oil-water interface on timescales of at least 10μs. These high speed boiling events are expected to be occuring at random points on the oil-water interface. A combination of such events could disrupt the full development of the momentum and thermal boundary layers. Even if the timescale of the bubbling events is 10μs, which is greater than the momentum diffusion time scale of 1μs, and the momentum boundary layer fully develops, this fast bubbling phenomena could cause diffusion to become important on average in the macro timescale of the droplet propelling on the oil film. In future research, the results could be confirmed with high speed videos taken from the bottom of the droplet.

With the fast bubbling events resetting the thermal and momentum boundary layers under the drop, the slopes in the momentum scaling equation can be replaced with linear approximations.

$$k\frac{\Delta T}{\Delta x_{cond}}\frac{1}{h_{fg}}V \sim \mu\frac{\Delta U}{\Delta x_{mom}} \tag{17}$$

$$\Delta x_{cond} \sim \delta_{cond} \tag{18}$$

$$\Delta x_{mom} \sim \delta_{mom} \tag{19}$$

Since the thermal and momentum boundary layers are assumed to be reset by the bubbles,

$$\Delta T \sim T_{surface} - T_{boil} \tag{20}$$

$$\Delta U \sim U \tag{21}$$

Substituting the results into the momentum equations for the slopes,

$$k\frac{\Delta T}{\delta_{cond}}\frac{1}{h_{fg}}V \sim \mu\frac{U}{\delta_{mom}} \tag{22}$$

Solving for U,

$$U \sim \frac{k}{\mu}\frac{\Delta T}{h_{fg}}V\frac{\delta_{mom}}{\delta_{cond}} \tag{23}$$

Note that

$$\frac{\delta_{mom}}{\delta_{cond}} \sim \sqrt{\frac{\mu c_p}{k}} \sim \sqrt{Pr} \tag{24}$$

Thus,

$$U \sim \frac{k}{\mu}\frac{\Delta T}{h_{fg}}V\sqrt{Pr} \sim \sqrt{\frac{kc_p}{\mu}}\frac{\Delta T}{h_{fg}}V \tag{25}$$

The $\mu^{-1/2}$ dependence of U appears again here. U is also independent of the thickness of the film and contact area between the droplet and oil film. Droplet velocities were measured at 140, 160, and 180°C with viscosities ranging from 189mPas to 13mPas. The largest and smallest droplet radii observed were 1.6 and 0.3mm, respectively. Figure 20 shows the experimental velocity plotted against the velocity predicted by the scaling model developed.

The experimental velocity data collapses onto the curve. The scaling captures the essential physics of the phenomena, and the model can accurately predict the velocity of a self-propelling droplet on a thin oil film. These results suggest that droplets are propelled by ejected vapor and opposed by viscous dissipation in the oil film below the droplet.

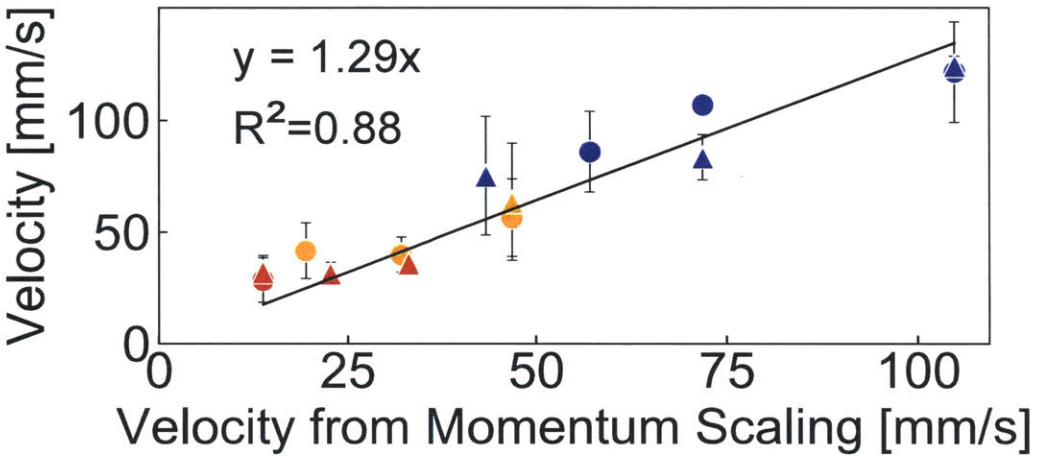

Figure 20: Experimental velocity vs model predicted velocity. The black line is a linear fit with the intercept forced to zero. Marker shape denotes surface type. Triangles indicate LIS and circles indicate flat, spincoated surfaces. Marker color denotes room temperature silicone oil viscosity. Blue, orange, and red indicate 100, 500, and 1,000cSt silicone oils, respectively.

4 Conclusion

In conclusion, the phenomenon of self-propelling droplets on thin liquid films was investigated. To the author's best knowledge, the phenomenon has not been studied before. This phenomena offers a promising alternative to other self-propelling methods explored previously because it requires minimal prior modification of the surface and no modification of impinging droplets. Knowledge of the phenomena may lead to improvements in self-cleaning surfaces, spray cooling, and anti-fouling surfaces.

After an initial heating stage, droplets exibited asymmetric bubbling and vapor ejection. The droplets quickly accelerated to a consistent velocity, independent of film thickness and droplet size, below a critical thickness and in a range of droplet sizes. The droplet velocity was found to scale as $\mu^{-0.5}$ implying that diffusion processes were significant in the oil film and that fast phenomena on timescales of order 1μs occur under the droplet to reset momentum and thermal diffusion in the oil film.

Fast surface fluctuations on timescales of at least 10μs were observed near the base and on the edge of boiling droplets. Evidence was presented of fluctuations at faster timescales. The fluctuations were attributed to fast bubbling occuring on the oil-water interface, which can reset the thermal and momentum boundary layers. A model scaling thin oil film viscous friction to the momentum of the vapor ejected from beneath the boiling droplet accurately predicts the experimental droplet velocities in a range of temperatures, viscosities, thicknesses, and droplet sizes indicating that the scaling captures the essential physics of the phenomena.

This work may be further developed with high speed imaging of propelling droplets from below and a study of the phenomena of the symmetry breaking process that results in the droplet propelling.

Bibliography

[1] Thomas M. Schutzius, Stefan Jung, Tanmoy Maitra, Gustav Graeber, Moritz Köhme, and Dimos Poulikakos. Spontaneous droplet trampolining on rigid superhydrophobic surfaces. *Nature*, 527:82, November 2015.

[2] James C. Bird, Rajeev Dhiman, Hyuk-Min Kwon, and Kripa K. Varanasi. Reducing the contact time of a bouncing drop. *Nature*, 503:385, November 2013.

[3] Katrina M. Wisdom, Jolanta A. Watson, Xiaopeng Qu, Fangjie Liu, Gregory S. Watson, and Chuan-Hua Chen. Self-cleaning of superhydrophobic surfaces by self-propelled jumping condensate. *Proceedings of the National Academy of Sciences of the United States of America*, 110(23630277):7992–7997, May 2013.

[4] Samantha McBride, Susmita Dash, and Kripa K. Varanasi. Evaporative crystallization in drops on superhydrophobic and liquid-impregnated surfaces. *Langmuir*, 34(41):12350–12358, October 2018.

[5] Periklis Papadopoulos, Lena Mammen, Xu Deng, Doris Vollmer, and Hans-Jürgen Butt. How superhydrophobicity breaks down. *Proc Natl Acad Sci USA*, 110(9):3254, February 2013.

[6] Karim S. Khalil, Seyed Reza Mahmoudi, Numan Abu-dheir, and Kripa K. Varanasi. Active surfaces: Ferrofluid-impregnated surfaces for active manipulation of droplets. *Appl. Phys. Lett.*, 105(4):041604, April 2014.

[7] H. Linke, B. J. Alemán, L. D. Melling, M. J. Taormina, M. J. Francis, C. C. Dow-Hygelund, V. Narayanan, R. P. Taylor, and A. Stout. Self-propelled leidenfrost droplets. *Phys. Rev. Lett.*, 96:154502, 2006.

[8] Edward Bormashenko, Yelena Bormashenko, Roman Grynyov, Hadas Aharoni, Gene Whyman, and Bernard P. Binks. Self-propulsion of liquid marbles: Leidenfrost-like levitation driven by marangoni flow. *The Journal of Physical Chemistry C*, 119(18):9910–9915, 2015.

[9] Nada Bjelobrk, Henri-Louis Girard, Srinivas Bengaluru Subramanyam, Hyuk-Min Kwon, David Quéré, and Kripa K. Varanasi. Thermocapillary

motion on lubricant-impregnated surfaces. *Phys. Rev. Fluids*, 1:063902, 2016.

[10] Ziane Izri, Marjolein N. van der Linden, Sébastien Michelin, and Olivier Dauchot. Self-propulsion of pure water droplets by spontaneous marangoni-stress-driven motion. *Phys. Rev. Lett.*, 113:248302, 2014.

[11] Masahide Gunji and Masao Washizu. Self-propulsion of a water droplet in an electric field. *Journal of Physics D: Applied Physics*, 38(14):2417–2423, 2005.

[12] G. Lagubeau, M. Merrer, C. Clanet, and D. Quere. Leidenfrost on a ratchet. *Nature Physics*, 7:395–398, 2011.

[13] Jeong Tae Ok, Eugene Lopez-Oña, Dimitris E. Nikitopoulos, Harris Wong, and Sunggook Park. Propulsion of droplets on micro- and submicron ratchet surfaces in the leidenfrost temperature regime. *Microfluidics and Nanofluidics*, 10(5):1045–1054, 2011.

[14] Yuejun Zhao, Fangjie Liu, and Chuan-Hua Chen. Thermocapillary actuation of binary drops on solid surfaces. *Applied Physics Letters*, 99(10):104101, 2011.

[15] P. de Gennes, F. Brochard-Wyart, and D. Quere. *Capillarity and Wetting Phenomena: Drops, Bubbles, Pearls, Waves.* Springer-Verlag New York, 2004.

[16] J. David Smith, Rajeev Dhiman, Sushant Anand, Ernesto Reza-Garduno, Robert E. Cohen, Gareth H. McKinley, and Kripa K. Varanasi. Droplet mobility on lubricant-impregnated surfaces. *Soft Matter*, 9:1772–1780, 2013.

[17] Yasuhiko H. Mori, Nobuhiko Tsui, and Masaaki Kiyomiya. Surface and interfacial tensions and their combined properties in seven binary, immiscible liquid-liquid-vapor systems. *Journal of Chemical & Engineering Data*, 29(4):407–412, 1984.

[18] Xi Yao, Yuhang Hu, Alison Grinthal, Tak-Sing Wong, L. Mahadevan, and Joanna Aizenberg. Adaptive fluid-infused porous films with tunable transparency and wettability. *Nature Materials*, 12:529, 2013.

[19] E. Ricci, R. Sangiorgi, and A. Passerone. Density and surface tension of dioctylphthalate, silicone oil and their solutions. *Surface and Coatings Technology*, 28(2):215–223, June 1986.

[20] Daniel Daniel, Max N. Mankin, Rebecca A. Belisle, Tak-Sing Wong, and Joanna Aizenberg. Lubricant-infused micro/nano-structured surfaces with tunable dynamic omniphobicity at high temperatures. *Appl. Phys. Lett.*, 102(23):231603, 2013.

[21] Clearco. Viscosity to Temperature Chart. `http://www.clearcoproducts.com/pdf/bath-fluids/silicone_fluids_viscosity_temp_chart.pdf`. Online; accessed 7-May-2019.

[22] DuPont. DuPont Krytox Performance Lubricants. `http://www2.dupont.com/Lubricants/en_US/assets/downloads/H-58510-5_Krytox_Typical_Properties.pdf`. Online; accessed 7-May-2019.

[23] J. Seiwert, C. Clanet, and D. Quere. Coating of a textured solid. *Journal of Fluid Mechanics*, 669:55–63, 2011.

[24] Chemours. DuPont Teflon AF Amorphous Fluoroplastic Resin. `https://www.chemours.com/Teflon_Industrial/en_US/assets/downloads/h44015.pdf`. Online; accessed 7-May-2019.

[25] Dan Daniel, Jaakko V. I. Timonen, Ruoping Li, Seneca J. Velling, and Joanna Aizenberg. Oleoplaning droplets on lubricated surfaces. *Nature Physics*, 13:1020, June 2017.

[26] Joseph W. Krumpfer and Thomas J. McCarthy. Rediscovering silicones: "unreactive" silicones react with inorganic surfaces. *Langmuir*, 27(18):11514–11519, September 2011.

[27] Alexander Eifert, Dorothea Paulssen, Subramanyan Namboodiri Varanakkottu, Tobias Baier, and Steffen Hardt. Simple fabrication of robust water-repellent surfaces with low contact-angle hysteresis based on impregnation. *Adv. Mater. Interfaces*, 1(3):1300138, April 2014.

[28] Alfred G. Emslie, Francis T. Bonner, and Leslie G. Peck. Flow of a viscous liquid on a rotating disk. *Journal of Applied Physics*, 29(5):858–862, April 1958.

[29] John H. Koschwanez, Robert H. Carlson, and Deirdre R. Meldrum. Thin pdms films using long spin times or tert-butyl alcohol as a solvent. *PLOS ONE*, 4(2):e4572, February 2009.

[30] D. L. Frost. Dynamics of explosive boiling of a droplet. *The Physics of Fluids*, 31(9):2554–2561, April 1988.

[31] Frank Schellenberger, Jing Xie, Noemí Encinas, Alexandre Hardy, Markus Klapper, Periklis Papadopoulos, Hans-Jürgen Butt, and Doris Vollmer. Direct observation of drops on slippery lubricant-infused surfaces. *Soft Matter*, 11(38):7617–7626, 2015.

[32] Martin Tress, Stefan Karpitschka, Periklis Papadopoulos, Jacco H. Snoeijer, Doris Vollmer, and Hans-Jürgen Butt. Shape of a sessile drop on a flat surface covered with a liquid film. *Soft Matter*, 13(20):3760–3767, 2017.

[33] Álvaro Moreno Soto, Tom Maddalena, Arjan Fraters, Devaraj van der Meer, and Detlef Lohse. Coalescence of diffusively growing gas bubbles. *Journal of Fluid Mechanics*, 846:143–165, 2018.

[34] F. H. Zhang and S. T. Thoroddsen. Satellite generation during bubble coalescence. *Physics of Fluids*, 20(2):022104, May 2008.